Biomedical Optics EXPRESS

Dynamics of cell and tissue growth acquired by means of extended field of view lensfree microscopy

F. Momey,[1,2,*] J.-G. Coutard,[1,2] T. Bordy,[1,2] F. Navarro,[1,2] M. Menneteau,[1,2] J.-M. Dinten,[1,2] and C. Allier[1,2]

[1] *Univ. Grenoble Alpes, F-38000 Grenoble, France*
[2] *CEA, LETI, MINATEC Campus, F-38054 Grenoble, France*
[*] *fabien.momey@cea.fr*

Abstract: In this paper, we discuss a new methodology based on lensfree imaging to perform wound healing assay with unprecedented statistics. Our video lensfree microscopy setup is a simple device featuring only a CMOS sensor and a semi coherent illumination system. Yet it is a powerful mean for the real-time monitoring of cultivated cells. It presents several key advantages, e.g. integration into standard incubator, compatibility with standard cell culture protocol, simplicity and ease of use. It can perform the follow-up in a large field of view (25 mm^2) of several crucial parameters during the culture of cells i.e. their motility, their proliferation rate or their death. Consequently the setup can gather large statistics both in space and time. Here we uses this facility in the context of wound healing assay to perform label-free measurements of the velocities of the fronts of proliferation of the cell layer as a function of time by means of particle image velocimetry (PIV) processing. However, for such tissue growth experiments, the field of view of 25 mm^2 remains not sufficient and results can be biased depending on the position of the device with respect to the recipient of the cell culture. Hence, to conduct exhaustive wound healing assays, we propose to enlarge the field of view up to 10 cm^2 through a raster scan, by moving the source/sensor with respect to the Petri dish. We have performed acquisitions of wound healing assay (keratinocytes HaCaT) both in real-time (25 mm^2) and in final point (10 cm^2) to assess the combination of velocimetry measurements and final point wide field imaging. In the future, we aim at combining directly our extended field of view acquisitions ($>$10 cm^2) with real time ability inside the incubator.

© 2016 Optical Society of America

OCIS codes: (170.0170) Medical optics and biotechnology; (170.1530) Cell analysis; (170.6935); (170.5810) Scanning microscopy; (170.6920) Time-resolved imaging; Tissue characterization; (090.0090) Holography; (090.1995) Digital holography.

References and links

1. C. Allier, S. V. Kesavan, J.-G. Coutard, O. Cioni, F. Momey, F. Navarro, M. Menneteau, B. Chalmond, P. Obeid, V. Haguet, B. David-Watine, S. Shorte, B. Van Der Sanden, C. Di Natale, L. Hamard, D. Wion, M. E. Dolega, N. Picollet-D'hahan, X. Gidrol, and J.-M. Dinten, "Video lensfree microscopy 2D and 3D culture of cells," Proc. SPIE **8947**, 89471H (2014).

#244089 Received 2 Jul 2015; revised 16 Sep 2015; accepted 24 Sep 2015; published 15 Jan 2016

2. S. V. Kesavan, F. Momey, B. David-Watine, N. Dubrulle, S. Shorte, E. Sulpice, D. Freida, B. Chalmond, J.-M. Dinten, X. Gidrol, and C. Allier, "High-throughput monitoring of major cell functions by means of lensfree video microscopy," Nature Scientific Reports **4**(5942) (2014).
3. S. Preibisch, S. Saalfeld, and P. Tomancak, "Globally optimal stitching of tiled 3D microscopic image acquisitions," Bioinformatics **25**(11), 1463–1465 (2009).
4. J. Schindelin, I. Arganda-Carreras, E. Frise, V. Kaynig, M. Longair, T. Pietzsch, S. Preibisch, C. Rueden, S. Saalfeld, B. Schmid, J.-Y. Tinevez, D. J. White, V. Hartenstein, K. W. Eliceiri, P. Tomancak, and A. Cardona, "Fiji: an open-source platform for biological-image analysis," Nature Methods **9**(7), 676–682 (2012).
5. C. A. Schneider, W. S. Rasband, and K. W. Eliceiri, "NIH Image to ImageJ: 25 years of image analysis," Nature Methods **9**, 671–675 (2012).
6. M. Poujade, E. Grasland-Mongrain, A. Hertzog, J. Jouanneau, P. Chavrier, B. Ladoux, A. Buguin, and P. Silberzan, "Collective migration of an epithelial monolayer in response to a model wound," Proc. Natl. Acad. Sci. USA **104**(41), 15988–15993 (2007).
7. M. Deforet, M. C. Parrini, L. Petitjean, M. Biondini, A. Buguin, J. Camonis, and P. Silberzan, "Automated velocity mapping of migrating cell populations (AVeMap)," Nature Methods **9**, 1081–1083 (2012).
8. T. W. Su, A. Erlinger, and A. Ozcan, "High-throughput lensfree imaging and characterization of a heterogeneous cell solution on a chip," Biotechnol. Bioeng. **102**(3), 856–868. (2009).
9. S. O. Isikman, W. Bishara, S. Mavandadi, F. W. Yu, S. Feng, R. Lau, and A. Ozcan, "Lens-free optical tomographic microscope with a large imaging volume on a chip," Proc. Natl. Acad. Sci. USA **108**(18), 7296-7301. (2011).
10. S. O. Isikman, A. Greenbaum, W. Luo, A. Coskun, and A. Ozcan, "Giga-pixel lensfree holographic microscopy and tomography using color image sensors," PLoS ONE **7**(9), e45044 (2012).
11. A. Greenbaum, W. Luo, T. W. Su, Z. Grcs, L. Xue, S. O. Isikman, A. F. Coskun, O Mudanyali, and A. Ozcan, "Imaging without lenses: achievements and remaining challenges of wide-field on-chip microscopy," Nature Methods **9**(9), 889–895. (2012).

1. Introduction

Lensfree imaging is a powerful tool for real-time, label-free monitoring of living cells. In previous works [1], we have demonstrated the potential of our lensfree video microscope (Fig. 1) to acquire images of cell cultures in Petri dishes directly inside a standard incubator, over periods going from a few hours to several days, with a temporal resolution of a few minutes. Our setup being devoid of any optical element (lenses, objectives), a large field of view (25 mm^2) is accessible, allowing to monitor about thousands of cells in a single image. Hence, we have been able to perform high-throughput label-free measurements and quantifications of major cell functions [2] (cell-substrate adhesion, cell spreading, cell division, cell death).

In the context of tissue growth experiments such as wound healing assays, lensfree imaging offers the possibility to follow and quantify the proliferation of a cell layer at the tissue's scale. We first address this point by measuring the velocities of the fronts of proliferation of the cell layer by means of particle image velocimetry (PIV) processing [6, 7] on lensfree sequences.

Still measurement biases could appear due to positioning the sensor at an irrelevant area. Hence it would be interesting to enlarge it again and be able to visualize the entire surface of proliferation of the cell culture, e.g. a Petri dish or a well plate. Consequently, we have developed a setup for addressing this challenging task. We have mounted the source/sensor couple on motorized XY stages, in order to acquire different positions of the field of interest. As a result we are able to scan and recombine in a single image the entire surface of interest, i.e. the entire available area for the proliferation of the seeded cell population (about 10-20cm^2), in about 10 minutes (scan + image recombination), with the same resolution as our first lensfree device. Our long-term objective is to couple extended field and real-time imaging inside the incubator on a single scanning device.

#244089 Received 2 Jul 2015; revised 16 Sep 2015; accepted 24 Sep 2015; published 15 Jan 2016
(C) 2016 OSA

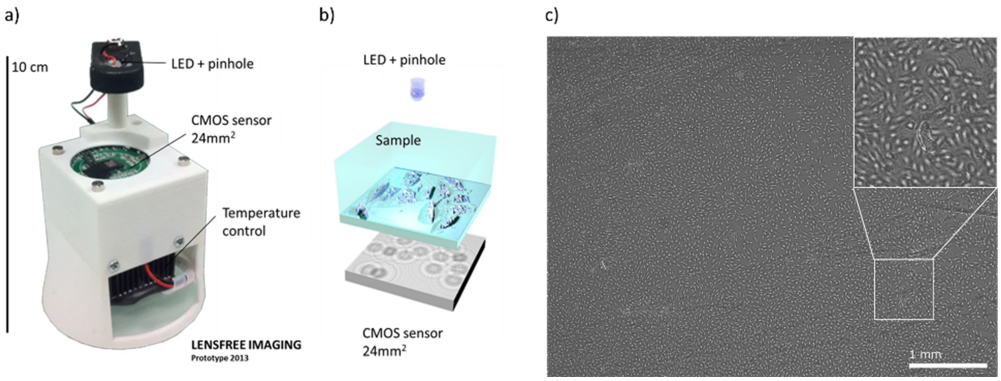

Fig. 1. (a) Experimental setup of the lensfree imaging device1. A CMOS image sensor is used for image acquisition and a LED and a 150μm pinhole for illumination (5cm above the image sensor). (b) The CMOS image sensor is put in contact with the Petri dish and records the holographic patterns resulting from the interference between the partially coherent incident light and the light scattered by the cells. Lensfree imaging is compatible with an incubation environment and can image 25 mm^2 of, e.g., a standard 35mm Petri dish. (c) The image shows the acquisition of approximately 8000 fibroblast cells acquired by means of the lensfree video microscope.

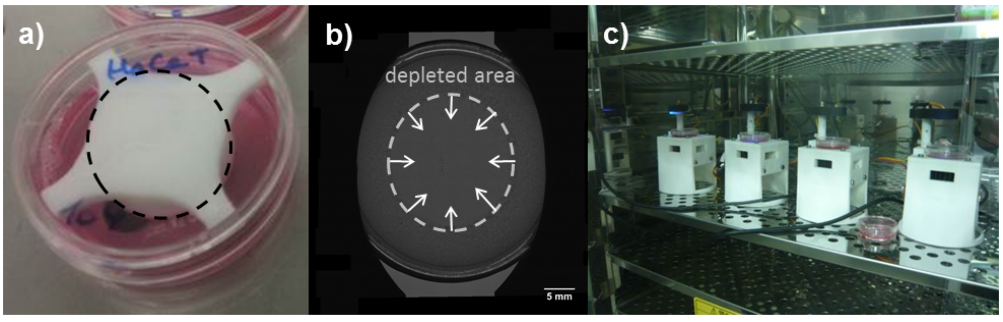

Fig. 2. (a) HaCaT culture in a Petri dish with a disk-shaped depletion plot (20mm). (b) Removing of the depletion plot at confluence. (c) Starting t0 of the growth experiment with real-time monitoring inside the incubator.

#244089 Received 2 Jul 2015; revised 16 Sep 2015; accepted 24 Sep 2015; published 15 Jan 2016
(C) 2016 OSA

2. Materials and methods

2.1. Experimental protocol

We seed the cells into a Petri dish. During this first step, a disk-shaped plot is positioned at the center of the dish in order to create the initial conditions of the growth experiment (Fig. 2(a)). This last will prevent the cells from growing in this zone. The plot is left into the Petri dish when it is put inside the incubator. Thus the cell layer grows all around the plot. At confluence, i.e. when all the non-depleted area is entirely occupied by the cell layer, the plot is removed (Fig. 2(b)). This is the starting point of the proper growth experiment: a crown of cells which will fill the left empty space, mimicking a wound healing. The Petri dish is put onto the lensfree video microscope which acquire images of a 25mm^2 area at the front of the cell layer, with a time step of 20 minutes (Fig. 2(c)). During a period of 96 hours, the culture colonize the disk-shaped freed surface. As a result, the proliferation front is a circle, allowing to have an unconstrained and isotropic proliferation of the cells. After 96 hours, the cell culture is removed from the incubator and we perform the acquisition of an image of whole the Petri dish thanks to our extended field lensfree scanner.

2.2. Lensfree video microscope

The video microscopy device is based on lensless imaging as described by Ozcan et al. [8, 9, 10, 11] which was modified to perform continuous monitoring in an incubator at a controlled temperature of 37 °C with humidity typically $> 80\%$ (Fig. 1). The device, and particularely the CMOS image sensor, was adapted to work in such extreme conditions (see appendix A). In a typical experiment, the lensfree video microscope is placed inside the incubator and the culture dish containing the cells is placed on top of the lensfree video microscope. The lensfree video microscope features a 12-bit Aptina MT9P031 CMOS RGB image sensor with a pixel pitch of 2.2 μm and an imaging area of 5.7×4.3mm^2. Illumination is provided by an LED along with a 150μm pinhole placed at a distance of approximately 5cm from the cells. The lensfree imaging setup does not acquire an image of the cell but a holographic interference pattern formed by the interference of the semi-coherent light scattered by the cell and the light passing directly from the source to the image sensor. The distance between the cells and the image sensor is not critical; for distances in the range of 0.5 mm up to 3 mm the 10-20 μm adherent cells provide holographic patterns with good signal-to-noise ratio. In our experiments, the typical distance between the cells and the image sensor is 1.2 mm.

2.3. Measurements of proliferation velocities by means of particle image velocimetry

For measuring the velocity of the front of proliferation as a function of time, we process the known PIV approach (Fig. 3(a) and 3(c)), already applied in the context of wound healing [6, 7]. PIV consists in determining the local shiftings map between 2 successive images of the sequence at dates t and $t+1$. The field of view is divided into patches of size $N \times N$ (typically 100×100 pixels). For each patch I^t and its successor I^{t+1} the correlation image C^t is calculated:

$$C^t = I^t * I^{t+1} \tag{1}$$

where $*$ designates the correlation operator. Each pixel of the correlation image C_t is then calculated as follows:

$$C^t_{ij} = C^t(i,j) = \sum_{m=1}^{N} \sum_{n=1}^{N} I^t(m,n) I^{t+1}(i+m, j+n) \tag{2}$$

The position of the spot of maximum intensity from the center C^t gives the local shifting. This method is applied to all images of the sequence. We assume that cell motility is the most relevant

#244089 Received 2 Jul 2015; revised 16 Sep 2015; accepted 24 Sep 2015; published 15 Jan 2016
(C) 2016 OSA

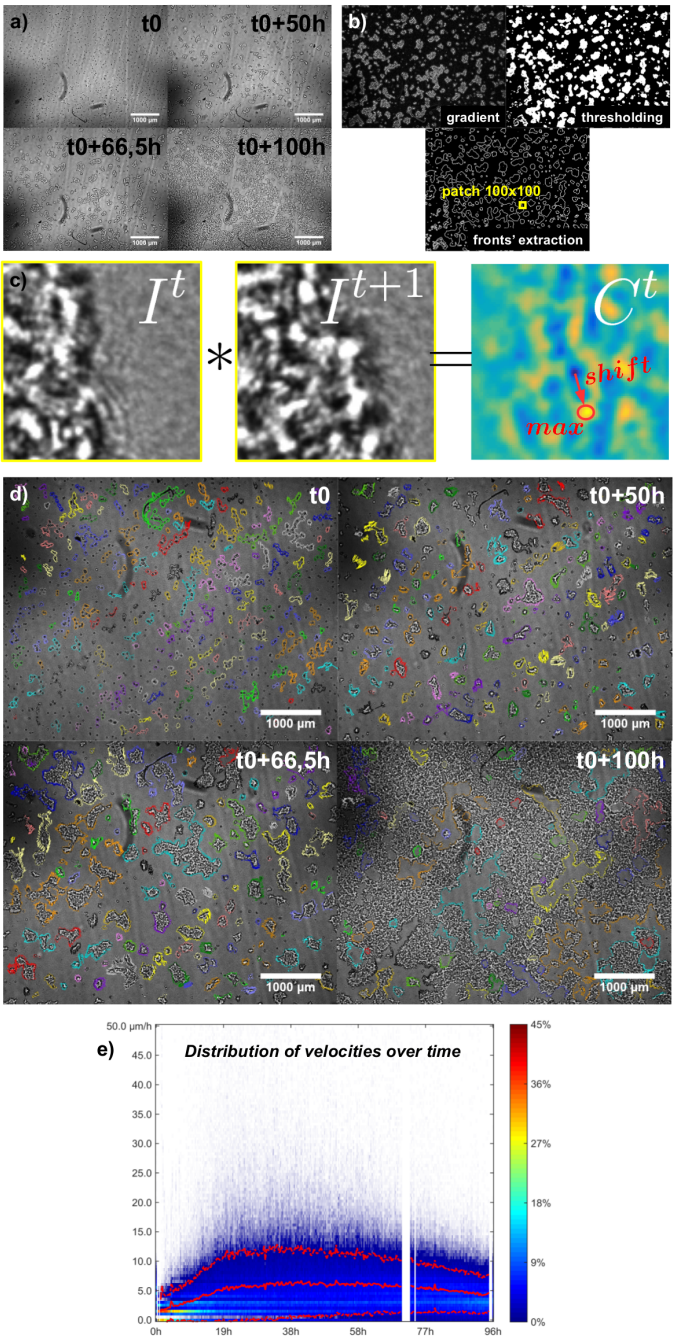

Fig. 3. (a) Real-time lensfree sequence of HaCaT cells' growth. (b) Image segmentation to get fronts positions. (c) PIV measurements of the front of proliferation. (d) PIV sequence of the front of proliferation (Visualization 1). The colors distinguish isolated fronts to visualize the progressive junctions of the cell layer. (e) Scatter plot of the distribution of velocities over time. The red curves corresponds to the mean velocity (solid) its standard deviation (dash). Blanks correspond to loss of acquisition. The colorbar identifies the concentration (in %) of calculated velocity vectors with a given speed value (ordinate axis in $\mu m/h$) at a given time (abscissa axis in hours).

#244089 Received 2 Jul 2015; revised 16 Sep 2015; accepted 24 Sep 2015; published 15 Jan 2016
(C) 2016 OSA

information that is extracted from PIV measurement. Thus we voluntailry neglect other factors that are caught by this method, such changes in cell adhesion, cell viability or cell morphology. These lasts are obviously sources of small errors in the absolute measurement of the velocity. A precise quantification of these errors is out of the scope of this paper. However we can briefly discuss the respective influence based on temporal and statistical considerations:

- In a normal experiment, cell adhesion varies mostly during cell division thus at a rate of approximately once every 20 hours, thus it will have a negligible effect on the PIV measurement.
- Cell viability is not such a problem since cell death is also reflected by a loss of motility. There will be a double negative effect on the PIV measurement.
- Cell morphology sounds more problematic since it can likely vary between 2 images. But the sensor resolution is too limited to catch the high frequency rings in the interference pattern that corresponds to the change in cell morphology. In other word unless the cell double its size between two images which is unlikely, we consider that there will be no influence on the PIV measurements.

In our case, we are only interested in the front motion. Thus we perform PIV on patches centered along the frontier that we find by appropriate segmentation of the images (Fig. 3(b)):

- Calculate the gradient image thanks to a Sobel filtering. As the cell layer looks textured on an almost "flat" background, this last is highlighted on a black background.
- Threshold the gradient image, thanks to a Kmeans thresholding algorithm, to keep only the highest gradients. We get a binary image of the segmented cell layer.
- Fill holes with a morphological closure operator in the segmented layer to get a binary image of the plain area occupied by the cells.
- Take the gradient image again: only the pixels belonging to the frontiers of the cell layer remain visible on the image.

Further we are able to quantify the local velocity of each point of the proliferations front all along the sequence (Fig. 3(d)). These measures of velocities are then performed on much larger, i.e. relevant areas than with classical microscopy ($\times 10$).

2.4. Extended field lensfree scanner

The extended field lensfree system is based on the same principle described in [1] and our previous setup (Fig. 1). Figure 4 shows our extended field lensfree setup. We have used 2 linear stages with 150mm range (Newport) set on XY configuration associated with an ESP300 motion controller. The sample is maintained on an adjustable Petri dish holder (Thorlabs ML-S203P2). The CMOS detector is an Aptina MT9J003 with a pixel pitch of 1.67μm measuring $6 \times 4.5\text{mm}^2$. It is packaged on a VFU USB camera board which is attached to the upper linear stage. In order to obtain more flexibility, the light source is here a lamp-fiber couple (white light LED), associated with a wavelength filter at 534 ± 42nm. The fiber has a diameter of 150μm and the output facet is placed at approximatively 5cm from the sample. The whole setup is piloted by a LabVIEW program: motion control, image snapping and saving. An acquisition consists in scanning a sample, e.g. a Petri dish, by configuring the XY motorized in snake mode, i.e. following a trajectory in "s" as shown in Fig. 5(a). The overlapping between 2 successive images is set at 20% in one direction so the entire area of interest is acquired by taking about 100 images in 5 minutes. The mosaic of images is then recombined (Fig. 5(b) and 5(c)) using

#244089 Received 2 Jul 2015; revised 16 Sep 2015; accepted 24 Sep 2015; published 15 Jan 2016
(C) 2016 OSA

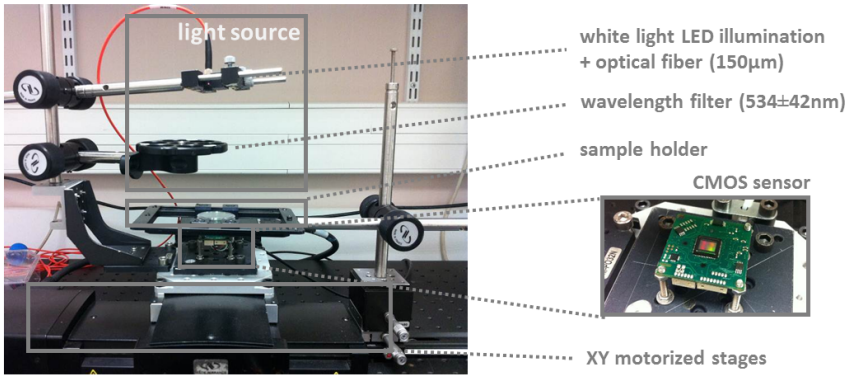

Fig. 4. Experimental setup of the lensfree scanner. The light source, a white light LED with optical fiber + a wavelength filter at 534 ± 42nm, and the CMOS sensor are mounted on 2 linear stages set on XY configuration. The sample holder remains static while the source/sensor couple is displaced by the XY stages following a snake-like trajectory in order to acquire the mosaic of images covering the entire area of interest.

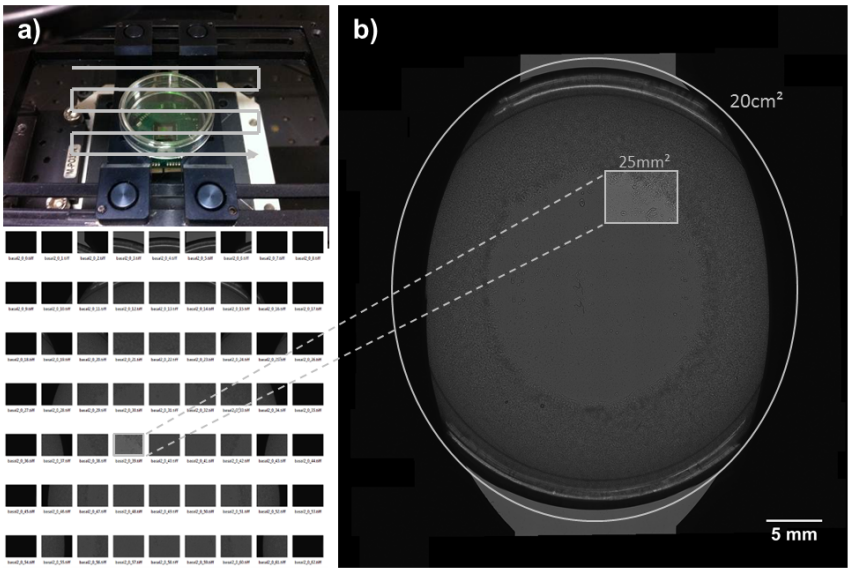

Fig. 5. (a) Scanning trajectory of a Petri dish containing a culture of HaCaT cells and the corresponding mosaic of acquired images. (b) Meta-image of the Petri dish recombined by the stitching plugin [3] of Fiji [4] (ImageJ [5]).

#244089 Received 2 Jul 2015; revised 16 Sep 2015; accepted 24 Sep 2015; published 15 Jan 2016
(C) 2016 OSA

a stitching plugin [3] available in the Fiji distribution [4] of the ImageJ [5] image processing program.

The stitching algorithm is obviously not perfect. It may badly recombine the images or even fail in this task. A reason could be the lack of information or a too important similarity between to successive images, yielding a wrong matching of the overlapping zones. As most of these algorithms are based on a maximisation of a correlation measurement between the overlapping zones, several solutions exist if the similarities are important.

However, as the trajectory of the scan is known, the position of each image of the mosaic is clearly identified. Of coursen, due the incertitudes of positioning of the motorized stages, these positions have to be refined by an algorithm but the task is clearly simplified.

Nevertheless, the refinement of the stitching algorithm is beyond the scope of this paper and would require further studies. In practice, the stitching algorithm we use gives us satisfactory results for quantifying the area of proliferation in our final point HaCaT growth experiment (section 3.2 and Fig. 7). According to our empirical observations, potential misregistration errors do not exceed few tens of microns on very localized areas. Moreover, a given experiment was not taken into account for the area measurements if the recombination of images clearly failed (which was quite rare). Thus all the experiments shown further were done on successful recombined images.

3. Results

3.1. Real-time velocities quantification

In our experimental protocol, the real-time lensfree sequence helps first monitoring the proper course of the cell proliferation, e.g. observing unexpected early cell death or stop of proliferation, or shrinking of the cell layer when the depletion plot was removed. Figure 6 shows 4 sequences corresponding to 4 different experiments. For each of them, we have measured the velocities along a front of proliferation as long as 5mm. The distribution of the velocity along the front and as a function of time results into a scatter (b, d, f, h) as illustrated in Fig. 3. The variations along the 5mm front are in the order of 90%. This huge variability demonstrates the interest brought by lensfree imaging to perform the velocities measurements on a sufficiently large field of view. We can observe a reproducible behavior of cell proliferation, with a monotonous decrease of the mean velocity from t0 to t0+96 hours, from 4.4 ± 4.6 μm/hours down to 2 ± 2.2 μm/hours in mean for the experiments (c), (e) and (g), and from 14.2 ± 7.2 μm/hours down to 6.9 ± 4.5 μm/hours for experiment (a). Note the higher velocity for the experiment (a) compared with the experiments (c), (e) and (g), which is another example of the possible wide variability of cell proliferations behavior in wound healing assays. The observed global decrease of the velocity for each experiment is mainly due to the fact that the culture medium is progressively consumed by the cells, decreasing the proliferation rate. Punctually, as identified by the red arrows on the graphs, we observe a sudden increase of the velocity which corresponds to the addition of culture medium.

3.2. Final point proliferation quantification

Figure 7 shows the meta-image of the final point acquisition which allows the measurement of the proliferation area of the entire cell culture from t0 to t0+96 hours. The measure is made easy by the fact that before the removing of the depletion plot at t0, the cell layer, constrained by the plot, start thickening. This yields to the apparition of a dark crown indicating the frontier of the depletion area (Fig. 7(a) and 7(b)). We can correlate this crown to the known diameter of the disk, giving the starting front of proliferation at t0 (Fig. 7(d) and 7(e)). Then we can delimit the new front of proliferation at t0+96 hours (Fig. 7(d) and 7(e)). The difference between the 2 delimited areas gives the area of proliferation (Fig. 7(g)). We found that taking the gradient

#244089 Received 2 Jul 2015; revised 16 Sep 2015; accepted 24 Sep 2015; published 15 Jan 2016
(C) 2016 OSA

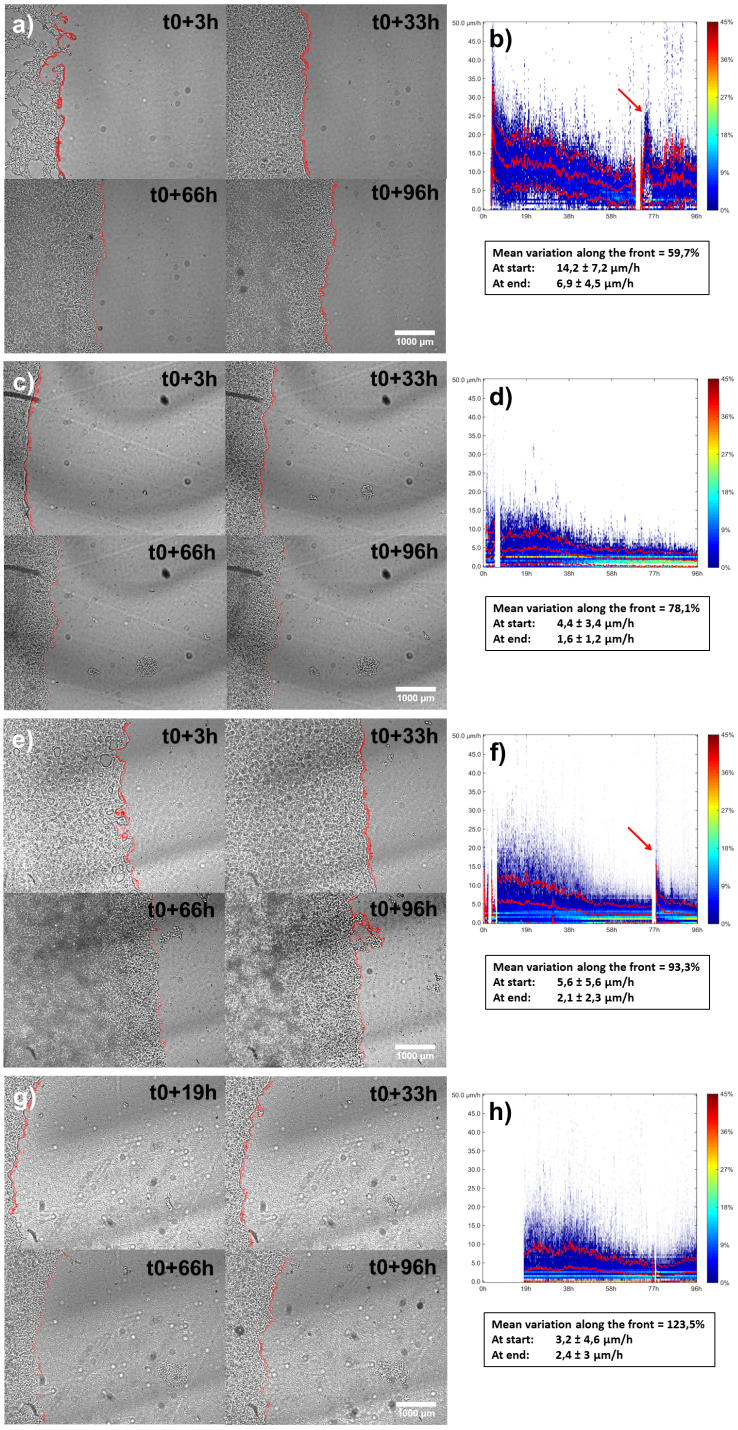

Fig. 6. Real-time lensfree sequences of 4 experiments (a, c, e, g) of HaCaT cultures (see Visualization 2, Visualization 3, Visualization 4, and Visualization 5) and their respective scatter graphs of distributions of proliferation velocities over time (b, d, f, h) as measured with PIV methods. The red curves corresponds to the mean velocity (solid) ± its standard deviation (dash). Blanks correspond to loss of acquisition. The red arrows on the graphs identify dates corresponding to the addition of culture medium.

#244089 Received 2 Jul 2015; revised 16 Sep 2015; accepted 24 Sep 2015; published 15 Jan 2016
(C) 2016 OSA

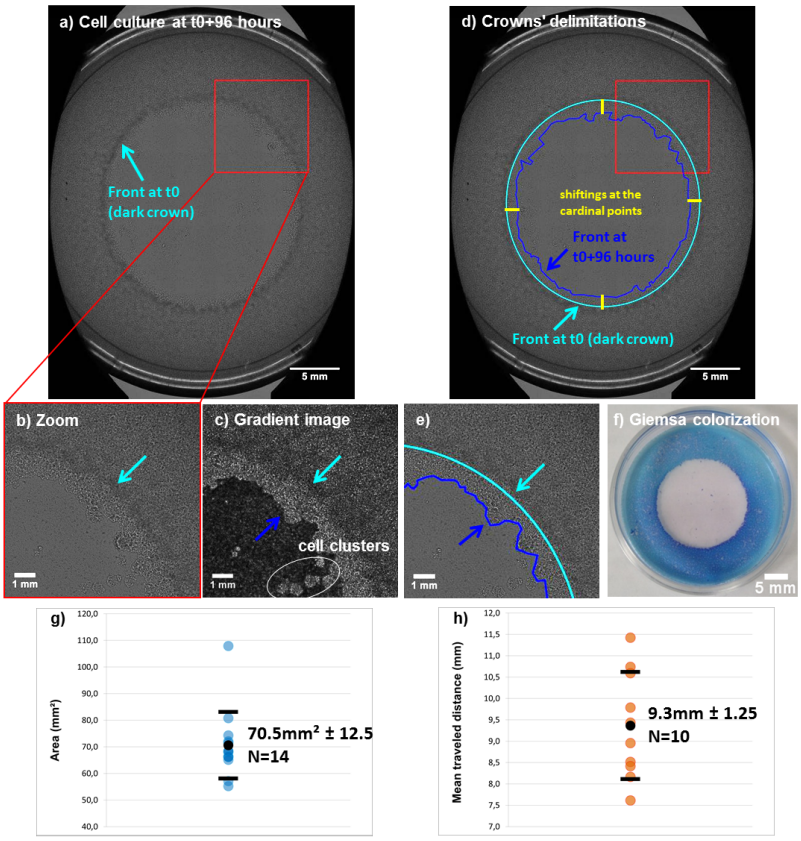

Fig. 7. Label-free measurement of the area of proliferation on the lensfree scan of the entire Petri dish of the HaCaT culture. (a) Meta-image at t0+96 hours. (b) Zoom on a region of interest. (c) Gradient image. The clusters corresponds to the growth of cells ripped at the removing of depletion plot. (d) Crowns' delimitations at t0 and t0+96 hours for areas' measurements. (f) Colorized Petri dish for classical non label-free measurements of proliferation. (g) Statistical results (mean and standard deviation) of quantification of the area of proliferation on $N = 14$ cell cultures (blue points). (h) Statistical results (mean and standard deviation) of quantification of the mean shifting at 4 cardinal points on $N = 10$ cell cultures (orange points).

#244089 Received 2 Jul 2015; revised 16 Sep 2015; accepted 24 Sep 2015; published 15 Jan 2016
(C) 2016 OSA

of the meta-image could offer an enhanced contrast and consequently a finer delimitation of the crown (Fig. 7(c)). On some experiments, we can see that some cells have colonized the depleted area and have grown without any connection to the initial crown, letting appear kinds of clusters. It is likely due to the removing of the depletion plot, which can tear off the initial cell layer and drop cells anywhere in the depleted area. When such clusters appear on the meta-image, we do not take them into account in our measurements because we are only interested in the proliferation of the cell layer. This method of measurement is very simple, and more important, label-free. Without the use of lensfree imaging, a classical biological protocol for performing such final point measurement, require fixing and colorizing the cells, to allow an empirical measure by an operator (Fig. 7(f)). We notice that the proliferation is not homogeneous over the crown. Hence, we also measure the shifting of the front at different points, e.g. the four "cardinal" points of the crown (Fig. 7(d)). As a result we get the mean shifting and the dispersion (standard deviation) of this parameter (Fig. 7(h)).

4. Conclusion

In this paper, we have reported a new methodology using real-time label-free lensfree imaging and PIV processing for quantifying the local velocities the proliferation fronts of a cell layer over a large field of view (25mm^2). Such measurements are performed on much larger areas in comparison with classical microscopy (x10) and can be followed over large periods of time. We have also reported a proof of concept of a extended field (10-20cm^2) lensfree scanner for imaging in cell biology. With such a device, we address the problem of a wrong positioning of the imaging system to an irrelevant field of view of the cell culture, by rapidly acquiring a meta-image of the entire area of interest with the same resolution as our known lensfree video microscopy device. We have tested our methodology on wound healing assays of cultures of keratinocytes HaCaT in Petri dishes. We coupled the scanning setup with real-time lensfree video microscopy (25mm^2) to monitor the experiments in time and get a measure of velocimetry (PIV) of the fronts of proliferation. These preliminary works have highlighted the great interest of combining in a single device, extended field of view fast acquisitions with real-time monitoring inside the incubator. In the future this configuration could extend lensfree imaging to real-time monitoring of very large containers for cell culture and high content experiments, such as well plates.

A. Hardware considerations for real-time lensfree imaging inside the incubator

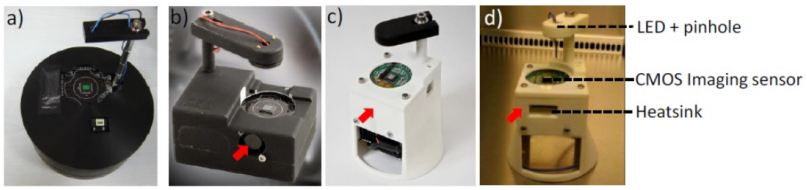

Fig. 8. Lensfree video microscope prototypes.(a) First lensfree video microscope prototype with a non-biocompatible exterior casing (Delrin - Polyoxymethylene). (b) Second prototype of lensfree video microscope, with a fan for ventilation (red arrow mark). Achievable temporal resolution is 15 minutes. The sensor is switched off in between image acquisitions. (c) Third prototype with Peltier element (red arrow), and an achievable temporal resolution close to 10 seconds. The imaging sensor is always on. (d) Lensfree video microscope where Peltier element is replaced by a heat-sink (red arrow), and opening for cross ventilation. The sensor is switched off in between acquisitions. Achievable temporal resolution is 15 minutes. All prototypes measure $\sim$ 10cm in height.

#244089 Received 2 Jul 2015; revised 16 Sep 2015; accepted 24 Sep 2015; published 15 Jan 2016
(C) 2016 OSA

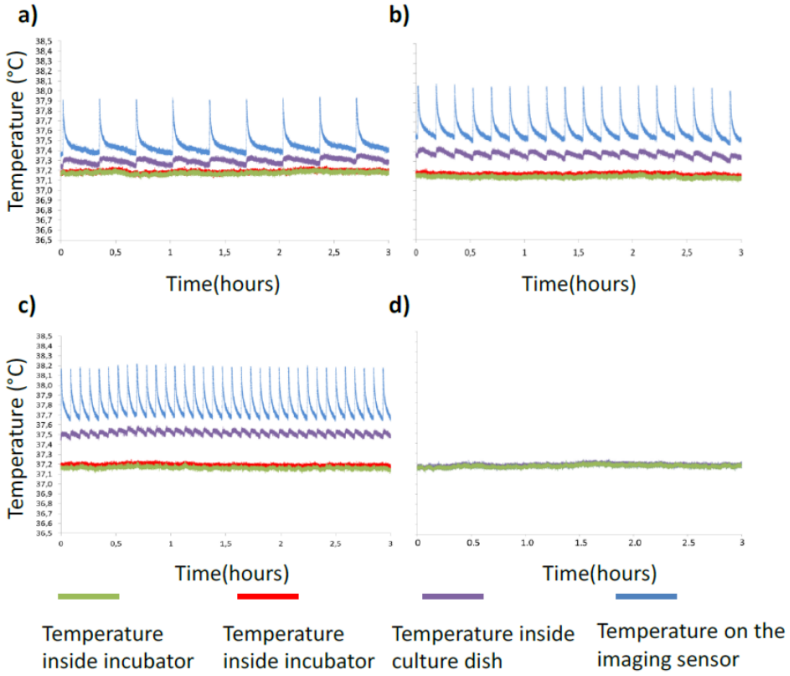

Fig. 9. Temperature increase and frequency of imaging. 4 temperature sensors were used for evaluation. 2 temperature sensors were placed inside the incubator at different points (lines green, red). The other 2 temperature sensors were placed inside the culture dish (line purple) and on top of the imaging sensor (line blue). (a,b,c) Temperature increase during image acquisitions is observed for temporal resolutions of 20 minutes, 10 minutes, and 5 minutes respectively. (d) Temperature stability of the lensfree video microscope, with integrated temperature control. It is to be noted that the temperature inside the culture dish placed on the system and the temperature inside the incubator do not vary.

To build a video microscope installable inside the standard incubator, we confronted major complications e.g. contamination of the cell culture, temperature stability and poor illumination condition due to diffusion in the culture medium. Our first prototype (Fig. 8(a)) caused major concerns due to a non-bio-compatible material, Polyoxymethylene (Delrin) used in the exterior casing, which emitted formaldehyde at very low concentration, yet enough to cause cell death. Another concern is that the imaging sensor and the associated circuit board get heated while being switched on continuously (up to 45°C from $\sim$ 20°C in $\sim$ 10 minutes). It is to be noted that the temperature inside the incubator is already at 37°C. Within initial 5 minutes the temperature of the imaging sensor and the circuit board (in continuous mode) surpasses 40°C. As a result, the temperature of the culture dish placed in contact with the imaging sensor increases, consequently resulting in cell death. Also, this causes evaporation of the culture media and subsequent condensation on the lid of the culture dish. This last point can be addressed by initially thermalizing the dish inside the incubator before putting it on the microscope and starting the acquisitions. In order to diminish the heating, (i) the imaging sensor is switched on only during image acquisitions (typically for 3 seconds), (ii) proper ventilation by a fan to minimize the temperature increase during acquisitions. These measures greatly minimized the heating, nullifying the evaporation of the culture media. Measurement of increase in temperature is shown while the lensfree video microscope acquires images with temporal resolution of 20 minutes (Fig. 9(a)) As it can be observed, the temperature on the sensor rises up to 37.9°C

#244089 Received 2 Jul 2015; revised 16 Sep 2015; accepted 24 Sep 2015; published 15 Jan 2016
(C) 2016 OSA

during image acquisitions (lasting typically 3 seconds), while the temperature inside the incubator is stable at 37.2°C. Immediately after image acquisition the temperature on the imaging sensor starts the descent and reaches 37.4°C in $\sim$ 8 minutes. However, the temperature increases inside the culture dish is lesser compared to the temperature increase on the imaging sensor. On an average, there is only a less than 0.1°C difference between the temperature inside the Petri dish and the temperature inside the incubator. However, if the frequency of imaging is increased to 1 image every 10 minutes (Fig. 9(b)) or every 5 minutes (Fig. 9(c)), a temperature difference of greater than 0.3°C is observed between the Petri dish and the incubator. Hence, our lensfree video microscope can offer only a limited temporal resolution of 15 minutes. For applications that require increased temporal resolution, a modification in the lensfree video microscopy setup is done to include a Peltier element to maintain the surface temperature of the imaging sensor at 37°C (Fig. 8(c)). This setup provides an increased temporal resolution of 10 seconds whilst maintaining the surface temperature at 37°C. Here, the temperature inside the culture dish placed on the imaging sensor is equal to the temperature inside the incubator (Fig. 9(d)). With this setup we have performed 1-minute longitudinal imaging of BJ cells inside standard incubator. However, using Peltier element is not satisfactory due to the cost involved ($\sim$ \$5000 Keithley Source-Measurement Unit AT 2510), and also due to the initial calibration ($\sim$ 3 hours) that is required to bring the imaging sensor temperature to a stable 37°C. Hence in our fourth prototype, we removed the Peltier element and replaced with a heat sink (Fig. 9(d)). Using this system, we obtain a temporal resolution of 15 minutes, which is suitable for myriad applications pertaining to cell biology.

#244089 Received 2 Jul 2015; revised 16 Sep 2015; accepted 24 Sep 2015; published 15 Jan 2016
(C) 2016 OSA